Journal of Inflammation Research

Dovepress
Taylor & Francis Group

Open Access Full Text Article

ORIGINAL RESEARCH

Quercetin, a Compound of the Total Flavonoids of *Periploca forrestii* Schltr., Ameliorates Rheumatoid Arthritis by Targeting TNF-α

Shuaishuai Chen[1,2,*], Weina Xue[1,3,*], Zhongxiu Wu[4,*], Dingyan Lu[1], Lin Zheng[1,5], Meng Zhou[1], Yongjun Li[1,5], Yonglin Wang[1,3], Ting Liu[1]

[1]State Key Laboratory of Discovery and Utilization of Functional Components in Traditional Chinese Medicine, Engineering Research Center for the Development and Application of Ethnic Medicine and TCM (Ministry of Education), Guizhou Provincial Engineering Research Center for the Development and Application of Ethnic Medicine and TCM, Guizhou Medical University, Guian New Area, 561113, People's Republic of China; [2]Guizhou Institute of Precision Medicine, Affiliated Hospital of Guizhou Medical University, Guiyang, 550009, People's Republic of China; [3]School of Pharmacy, Guizhou Medical University, Guian New Area, 561113, People's Republic of China; [4]Department of Pharmacy, Zhejiang Provincial People's Hospital Bijie Hospital, Bijie, 551799, People's Republic of China; [5]National Engineering Research Center of Miao's Medicines, Guiyang, 550004, People's Republic of China

*These authors contributed equally to this work

Correspondence: Yongjun Li; Ting Liu, State Key Laboratory of Discovery and Utilization of Functional Components in Traditional Chinese Medicine, Engineering Research Center for the Development and Application of Ethnic Medicine and TCM (Ministry of Education), Guizhou Provincial Engineering Research Center for the Development and Application of Ethnic Medicine and TCM, Guizhou Medical University, 6, Ankang Avenue, Guian New Area, 561113, People's Republic of China, Tel +86 0851-86908468, Email liyongjun026@126.com; liuting@gmc.edu.cn

Objective: The total flavonoids of *Periploca forrestii* Schltr. (TFPF) exhibit notable anti-rheumatoid arthritis (RA) properties, highlighted by their inhibitory action on TNF-α. This study investigates the specific compounds of TFPF responsible for TNF-α inhibition and delineates their mechanism of action.

Methods: L929 cells and luciferase-based assays were used to assess anti-TNF-α activity. Additionally, MH7A cells and Wistar rats were employed to establish in vitro and in vivo models of RA. Chemical chromatography, thermal proteome profiling (TPP), molecular docking, surface plasmon resonance (SPR), cellular thermal shift assays (CETSA), drug affinity responsive target stability tests (DARTS), and transcriptomic analysis were used to study the potent molecules of TFPF and their protein targets and pathways. H&E staining, immunofluorescence staining, ELISA, and Western blot were employed for pharmacodynamic and mechanism studies of these potent molecules.

Results: TFPF mitigated cellular injury in L929 cells and inhibited luciferase expression, both of which were induced by TNF-α. Among the eight compounds identified, quercetin exhibited the most potent anti-TNF-α activity. Quercetin improved cellular injury and reduced the cell apoptosis rate in L929 cells treated with TNF-α. TPP revealed the interaction between quercetin and TNF-α, which was verified by molecular docking, SPR, CETSA, and DARTS assays. Transcriptomic analysis highlighted the TNF signaling pathway, suggesting that quercetin may target TNF-α to inhibit the activation of the NF-κB signaling pathway. Quercetin inhibited luciferase expression, suppressed the phosphorylation of IκBα and p65, blocked p65 nuclear translocation, and reduced the mRNA expression of *COX-2, INOS, IL-6*, and *IL-1β*. Moreover, quercetin decreased inflammation and joint damage in RA.

Conclusion: Quercetin, a compound of TFPF, interacts with and inhibits the activity of TNF-α, thereby suppressing the TNF-α/NF-κB signaling pathway and alleviating the symptoms of RA. These findings position quercetin as a promising TNF-α inhibitor for the treatment of RA.

Keywords: TNF-α inhibitor, quercetin, total flavonoids of *Periploca forrestii* Schltr., rheumatoid arthritis, molecular interaction techniques, binding ability

Received: 20 September 2024
Accepted: 9 February 2025
Published: 26 February 2025

Graphical Abstract

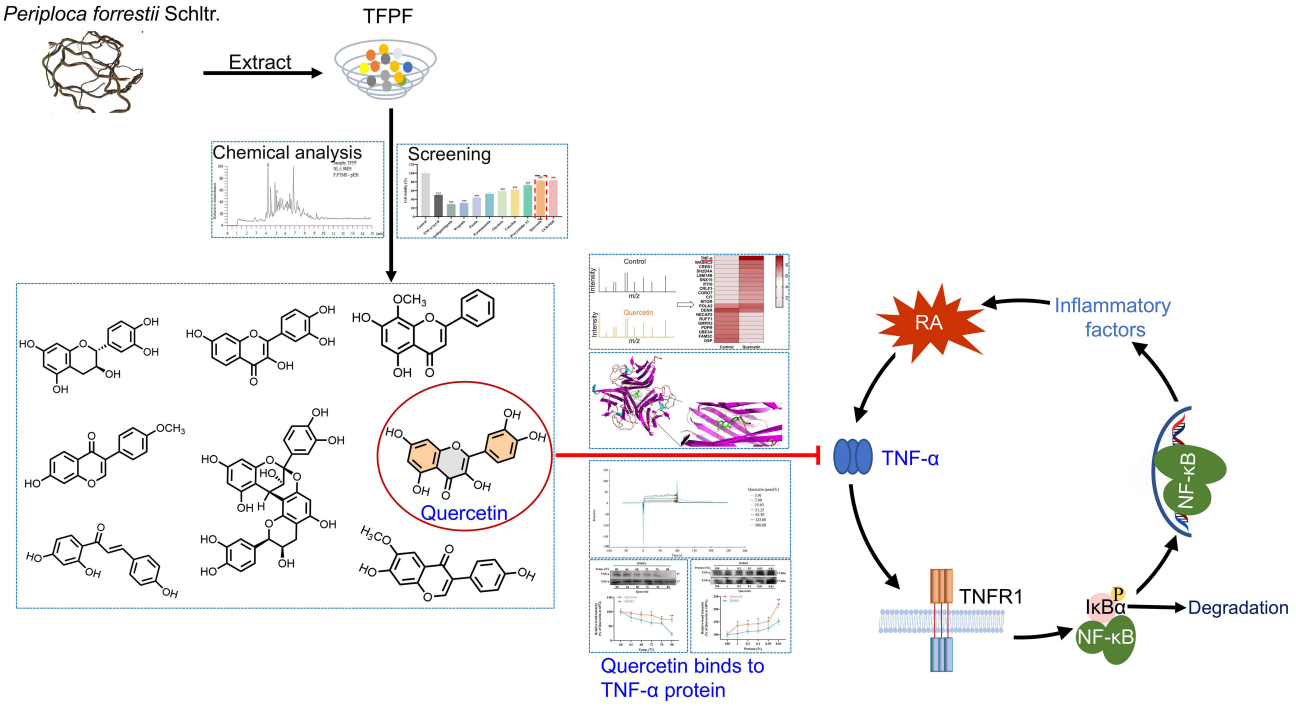

Introduction

Rheumatoid arthritis (RA) is a systemic, chronic inflammatory autoimmune disorder characterized by the proliferation of synovial tissue, pannus formation, and progressive erosion of cartilage.[1] The condition is marked by extended treatment periods, substantial healthcare costs, and a high likelihood of recurrence.[2,3] Recent statistics reveal a 0.46% increase in RA prevalence since 2019,[4] coupled with elevated mortality rates among RA patients compared to the general population.[5] These findings highlight RA as a significant public health issue.

Tumor necrosis factor-alpha (TNF-α), a crucial cytokine within the TNF superfamily, plays a pivotal role in the onset and exacerbation of various autoimmune conditions, including RA, psoriasis, multiple sclerosis, and Crohn's disease.[6] TNF-α primarily interacts with the tumor necrosis factor receptor 1 (TNFR1), which possesses an intracellular death domain, leading to the formation of the TNFR1 signaling complex.[6,7] This complex activates the inhibitor of nuclear factor-kappa B kinase, catalyzing the phosphorylation, ubiquitination, and subsequent degradation of the inhibitor of NF-κB α (IκBα).[8] The degradation of IκBα permits the translocation of NF-κB into the nucleus, where it initiates the transcription of pro-inflammatory cytokines such as TNF-α, interleukin-6 (IL-6), and interleukin-1β (IL-1β), thereby driving the inflammatory processes characteristic of RA. Despite the availability of several anti-TNF-α biologics, such as infliximab, adalimumab, and golimumab, which have significantly improved RA management,[9] their use is often limited by issues such as drug resistance, high treatment costs, and severe adverse effects.[10] There is thus a pressing need for the development of natural TNF-α inhibitors that combine efficacy with reduced toxicity, offering a promising strategy to effectively control RA symptoms.

Periploca forrestii Schltr. (PF, known as Heiguteng in Chinese) is traditionally used to dredge meridians, dispel wind, and alleviate dampness. It is commonly incorporated in RA treatments and is widely distributed in China, India, Myanmar, and other regions.[11,12] PF is well known for its diverse pharmacological activities, including anti-inflammatory, anti-arthritic, antioxidant, and antitumor effects.[11] It is commonly utilized through methods such as water soaking, wine infusion, and decoction to meet diverse medicinal and edible needs. Previous research has

demonstrated that a 70% ethanol extract of PF significantly reduces RA symptoms.[12] Our integrative approach, which combines network pharmacology with experimental validation, has identified TNF-α as a central therapeutic target of PF, highlighting its potential benefits in RA treatment.[13] Subsequent fractionation of the 70% ethanol extract revealed that the total flavonoids of PF (TFPF) are a particularly active component against RA. However, the specific anti-TNF-α functional compounds of TFPF and their molecular mechanisms remain unexplored.

In this study, we systematically screened and identified the functional compounds of TFPF that exhibit anti-TNF-α activity. To determine and validate the protein targets of these compounds, we integrated several advanced techniques, including thermal proteome profiling (TPP), molecular docking, surface plasmon resonance (SPR), cellular thermal shift assay (CETSA), and drug affinity responsive target stability (DARTS). Transcriptomic analysis was used to delineate the signaling pathways influenced by the interaction of these candidate compounds with their respective protein targets. Additionally, a luciferase-based reporter gene assay, in conjunction with MH7A cells, provided empirical support for the transcriptomic findings. Lastly, the therapeutic potential of these compounds against RA was evaluated using a collagen-induced arthritis (CIA) rat model, providing a comprehensive assessment of their efficacy.

Materials and Methods

Reagents and Antibodies

Dulbecco's modified Eagle medium (DMEM; C11995500BT, Thermo Fisher), Roswell Park Memorial Institute (RPMI) 1640 medium (C11875500BT, Thermo Fisher), fetal bovine serum (FBS; 16140071, Thermo Fisher), FuGENE® 6 transfection reagent (E2692, Promega), CellTiter 96® AQueous One Solution reagent (G3582, Promega), Eastep® Super Total RNA Extraction Kit (LS1040, Promega), Nano-Glo® Luciferase Assay System (N1110, Promega), pNL3.2.NF-κB-RE [NlucP/NF-κB-RE/Hygro] plasmid (N111, Promega), TNF-α protein (300–01A, PeproTech Inc.), bovine serum albumin (BSA; IA0910, Solarbio Technology Co., Ltd.), Triton X-100 (T8200, Solarbio Technology Co., Ltd.), protein marker (abs923, Absin Bioscience Inc.), phenylmethanesulfonyl fluoride (PMSF; ST506, Beyotime), radioimmunoprecipitation assay (RIPA) lysis buffer (P0013B, Beyotime), enhanced chemiluminescence kit (P0018S, Beyotime), PrimeScript™ RT Master Mix kit (RR036A, Takara Bio Inc.), FITC Annexin V Apoptosis Detection kit (556547, BD Biosciences), UCB-9260 (HY-133122, MedChemExpress), rutin (≥ 98.0%, CAS no. 153-18-4, Guizhou Dida Biology), fisetin (≥ 98.0%, CAS no. 528-48-3, ABPHYTO), glycitein (≥ 98.0%, CAS no. 40957-83-3, ABPHYTO), formononetin (≥ 98.0%, CAS no. 485-72-3, ABPHYTO), procyanidin A2 (≥ 98.0%, CAS no. 41743-41-3, ABPHYTO), quercetin (≥ 99.1%, CAS no. 117-39-5, National Institutes for Food and Drug Control), wogonin (CAS no. 632-85-9, National Institutes for Food and Drug Control), catechin (≥ 97.0%, CAS no. 154-23-4, Shanghai Aladdin Biochemical Technology Co., Ltd.), isoliquiritigenin (≥ 98.0%, CAS no. 961-29-5, Shanghai Aladdin Biochemical Technology Co., Ltd.), methotrexate (MTX; ≥ 98.0%, CAS no. 59-05-2, InnoChem Science & Technology Co., Ltd.), actinomycin D (Act-D; GC16866, GlpBio Technology Inc.), Pronase enzyme (GC30124, GlpBio Technology Inc.), lipopolysaccharides (LPS; L2880, Sigma-Aldrich), incomplete Freund's adjuvant (F5506, Sigma-Aldrich), Rat TNF-α enzyme-linked immunosorbent assay (ELISA) Kit (ZC-37624, ZCIBIO Technology Co., Ltd.), Rat rheumatoid factor (RF) ELISA Kit (ZC-36930, ZCIBIO Technology Co., Ltd.), Rat IL-6 ELISA Kit (ZC-36404, ZCIBIO Technology Co., Ltd.), Rat IL-1β ELISA Kit (ZC-36391, ZCIBIO Technology Co., Ltd.), and bovine type II collagen (20022, Chondrex) were purchased from their respective manufacturers. Mouse anti-glyceraldehyde-3-phosphate dehydrogenase (GAPDH; MA5-15738, Thermo Fisher), goat anti-rabbit (31460, Thermo Fisher), goat anti-mouse IgG (31430, Thermo Fisher), rabbit anti-p65 (8242S, Cell Signaling Technology), rabbit anti-phosphorylated p65 (p-p65; 3033S, Cell Signaling Technology), rabbit anti-IκBα (4812S, Cell Signaling Technology), and rabbit anti-phosphorylated IκBα (p-IκBα; 2859S, Cell Signaling Technology) were also obtained from their respective manufacturers.

Preparation and Determination of the Total Flavonoid Content of PF Extract and TFPF

PF was procured from the Bird and Flower Market in Guiyang and authenticated by A.P. Chunhua Liu from Guizhou Medical University, China. A voucher specimen (GY20200506) is deposited in the Herbarium of the State Key Laboratory of Discovery and Utilization of Functional Components in Traditional Chinese Medicine. The raw material

was subjected to a sequential extraction process using 70% ethanol, with successive solid-to-solvent ratios of 1:8, 1:6, and 1:6. Each extraction phase lasted 1 hour and 30 minutes under reflux conditions. The resultant solutions from each phase were combined and concentrated using a rotary vacuum evaporator to yield a dry PF extract.

The PF extract was then reconstituted in an appropriate volume of distilled water and subjected to a triple liquid-liquid extraction using equal volumes of ethyl acetate. The collected organic layers were further concentrated under reduced pressure and purified using D101 macroporous resin, followed by elution with 70% ethanol to obtain the final TFPF powder.

The quantification of total flavonoids in PF extract and TFPF was performed using the aluminum nitrate-sodium nitrite colorimetric method, as described by Liu et al.[14] The flavonoid content was calculated based on a calibration curve established with rutin as the standard.

Cell Culture and Cell Viability Assay

L929 and HEK293T cells were sourced from the National Collection of Authenticated Cell Cultures, Shanghai, China. MH7A cells were acquired from Jennio Biological Technology, Guangzhou, China, and RAW264.7 macrophages were obtained from the American Type Culture Collection, MD, USA. All cell lines were maintained in DMEM or RPMI 1640 medium supplemented with 10% FBS. Cells were cultured in a humidified incubator at 37°C and 5% CO_2. After treatment, cell viability was assessed using the MTS assay.

Determination of Tolerable Concentrations

To establish the tolerable concentration ranges for PF extract, TFPF, and quercetin, cell viability assays were conducted across multiple cell lines. L929, HEK293T and MH7A cells were seeded at a density of 1.5×10^5 cells/mL in 96-well plates. L929 cells were exposed to PF extract and TFPF at concentrations of 0, 25, 50, 100, 250, and 500 ng/mL, and to quercetin at 0, 5, 10, 15, 25, 50, and 100 μmol/L for 12 hours. HEK293T cells were similarly treated with the same concentrations of PF extract, TFPF, and with reduced concentrations of quercetin (0, 5, 10, 15, 25, and 50 μmol/L) for 5 hours. Concurrently, MH7A cells were tested with quercetin concentrations ranging from 0 to 100 μmol/L for 24 hours. These assays were designed to determine the maximum non-toxic concentrations of each compound, ensuring safety margins for subsequent therapeutic studies.

Determination of Anti-TNF-α Activity

A TNF-α-induced L929 cell death model was employed to assess anti-TNF-α activity. L929 cells were treated with PF extract (0–100 ng/mL), TFPF (0–100 ng/mL), and eight identified compounds (fisetin, glycitein, isoliquiritigenin, formononetin, wogonin, catechin, procyanidin A2, and quercetin; each at 50 μmol/L), as well as varying concentrations of quercetin (0–50 μmol/L), all in the presence of TNF-α (7.5 ng/mL) and Act-D (0.5 μg/mL) for 12 hours. UCB-9260 (10 μmol/L) was used as a positive control under similar conditions.

Luciferase Expression Assay

HEK293T cells in the logarithmic phase (1.5×10^5 cells/mL) were plated in 96-well plates and transfected with FuGENE® 6 transfection reagent and the pNL3.2.NF-κB-RE [NlucP/NF-κB-RE/Hygro] plasmid at a volume ratio of 3:1 to construct NlucP-NF-κB-HEK293T cells.

NlucP-NF-κB-HEK293T cells were plated at a density of 1.5×10^5 cells/mL and treated with PF extract (0–500 ng/mL), TFPF (0–500 ng/mL), quercetin (0–15 μmol/L), or UCB-9260 (10 μmol/L; positive control) at various concentrations, in the presence or absence of TNF-α (20 ng/mL), for 5 hours. Luciferase expression, indicative of NF-κB activity, was measured using the Nano-Glo® Luciferase Assay System and expressed as relative light units (RLU) normalized to the control group.

UHPLC-Q-Exactive Orbitrap HRMS Analysis

TFPF was prepared by ultrasonication in methanol, followed by centrifugation at 12,000 × *g* for 10 minutes to clarify the solution. The supernatant was filtered through a 0.22 μm membrane prior to analysis to ensure purity. The analysis of the

flavonoids—fisetin, glycitein, isoliquiritigenin, formononetin, wogonin, catechin, procyanidin A2, and quercetin—was conducted using a UHPLC-Q-Exactive Plus Orbitrap HRMS (Thermo Fisher Scientific, Waltham, MA, USA).

Chromatographic separation was achieved on a Hypersil GOLD™ C18 column (100 × 2.1 mm, 1.9 μm) with a mobile phase consisting of water with 0.1% formic acid (A) and acetonitrile with 0.1% formic acid (B). The elution gradient was set as follows: 0–7 minutes, 5% B; 7–18 minutes, 5–70% B; 18–19.5 minutes, 70–95% B; and 19.5–24 minutes, 5% B. The flow rate was maintained at 300 μL/min, and the column temperature was controlled at 40°C. Sample injections were 5 μL.

The mass spectrometry conditions included a spray voltage of 3.8 kV (+) / 2.5 kV (-), a vaporizer temperature of 350°C, sheath gas at 35 arb, auxiliary gas at 10 arb, and a capillary temperature of 320°C. The instrument was operated in a full MS/dd-MS^2 mode with a scan range from 100 to 2,000 *m/z*, achieving a resolution of 7,000 for MS^1 and 15,000 for MS/MS with stepped NCE settings of 20, 40, and 60. Data analysis was conducted using Xcalibur software.

Cell Morphology Observation

L929 cells were seeded at a concentration of 1.5×10^5 cells/mL in 6-well plates and treated with quercetin at concentrations of 0, 15, 25, and 50 μmol/L or UCB-9260 at 10 μmol/L, either in the presence or absence of TNF-α (7.5 ng/mL) and Act-D (0.5 μg/mL) for 12 hours. After treatment, cellular morphology was examined using an inverted microscope to identify morphological alterations.

Apoptosis Rate Determination

Following treatment, apoptosis was quantified using the Annexin V-FITC/PI staining protocol. L929 cells were washed twice with phosphate buffered saline (PBS) and dissociated using trypsin without EDTA. The cells were then dual-stained with 5 μL of PI and 5 μL of FITC-Annexin V. A BD C6 Plus flow cytometer was used to analyze the cells.

TPP Analysis

MH7A cells were cultured to a density of 1.5×10^5 cells/mL, washed twice with ice-cold PBS, and lysed in RIPA buffer supplemented with 1% PMSF. The cell lysates were then centrifuged at 12,000 rpm for 20 minutes at 4°C. The supernatant, containing the protein extract, was treated with either dimethyl sulfoxide (DMSO) as a control or 80 μmol/L quercetin for 30 minutes at room temperature. The samples were then heated to 72°C for 3 minutes for subsequent TPP analysis. Proteins with a log2 fold change exceeding ±2, a statistical significance *p*-value below 0.05, and the detection of at least two unique peptides per protein were classified as differentially expressed proteins (DEPs). Kyoto Encyclopedia of Genes and Genomes (KEGG) pathway analyses were performed using the KEGG Orthology Based Annotation System.

Molecular Docking

The three-dimensional structure of TNF-α was retrieved from the Protein Data Bank, and the molecular structure of quercetin was obtained in mol2 format from ZINC15. Data were prepared using AutoDock Tools 1.5.6 and visualized with PyMOL 2.3.0. Docking simulations were performed using AutoDock Vina 1.1.2, and results were analyzed using PyMOL 2.3.0.

SPR for the Binding Effect of Quercetin and TNF-α

Quercetin was dissolved in DMSO using ultrasonic equipment and then diluted in PBS (v/v, containing 5% DMSO). The final concentration of quercetin was set as 3.91, 7.80, 15.63, 31.25, 62.50, 125.00, and 500.00 μmol/L. The samples were analyzed using a Biacore X100 (Cytiva Sweden AB, Uppsala, Sweden), and binding curves were generated using Biacore X100 Evaluation Software. The SPR parameters were set as follows: the flow rate was set at 30 μL/min; the binding time was 100 seconds; and the dissociation time was 150 seconds.

CETSA for TNF-α-Quercetin Binding Activity

RAW264.7 cells treated with LPS (1 μg/mL) for 24 hours were lysed following washing with ice-cold PBS. Cell lysates were treated with DMSO or quercetin (80 μmol/L) for 30 minutes at room temperature. Samples were heated at various temperatures (60–80°C) for 3 minutes and then centrifuged at 12,000 rpm for 10 minutes at 4°C. The supernatants were analyzed by Western blot.

DARTS Assay for Quercetin Binding to TNF-α

Cell lysates from RAW264.7 cells treated with DMSO or quercetin (80 μmol/L) were divided into six aliquots and incubated with varying concentrations of pronase (1 μL of each; 100%, 1%, 0.3%, 0.1%, 0.03%, and 0.01%) for 30 minutes at room temperature. Pronase activity was halted by adding a pronase enzyme inhibitor (1 μL per sample). The proteins were then subjected to Western blot analysis.

Transcriptomic Analysis

MH7A cells (1.5×10^5 cells/mL) were treated with TNF-α (30 ng/mL) in the presence or absence of quercetin (1.5 μmol/L) for 24 hours. RNA was extracted using TRIzol reagent and analyzed by Applied Protein Technology Co., Ltd. (Shanghai, China). Differentially expressed genes (DEGs) were identified using a significance threshold of $p < 0.05$ and an absolute $\log_2$ (fold change) greater than 1.

Western Blot Analysis

MH7A cells, plated at 1.5×10^5 cells/mL in a 6-well plate, were treated with varying concentrations of quercetin (0, 0.5, 1, and 1.5 μmol/L). The cells were lysed using RIPA buffer containing 1% PMSF, and the lysates were centrifuged at 12,000 rpm for 10 minutes at 4°C. Protein concentrations were determined using a BCA protein assay kit. Proteins (10 μg per sample) were separated by sodium dodecyl sulfate–polyacrylamide gel electrophoresis and transferred to polyvinylidene fluoride membranes. The membranes were blocked with 5% BSA for 3 hours at room temperature, incubated overnight at 4°C with primary antibodies against IκBα, p-IκBα, p65, and p-p65 (1:1,000 dilution), followed by a 2-hour incubation with horseradish peroxidase-conjugated secondary antibody (1:2,000). Band intensity was quantified using Quantity One software and normalized to GAPDH.

p65 Nuclear Translocation Assay

MH7A cells were cultured at 1.5×10^5 cells/mL and treated with various concentrations of quercetin (0, 0.5, 1, and 1.5 μmol/L) in the presence or absence of TNF-α (30 ng/mL) for 24 hours. After treatment, the cells were fixed with 4% formaldehyde and permeabilized with 0.5% Triton X-100 for 20 minutes. Non-specific binding was blocked using 5% BSA for 30 minutes. The cells were then incubated with a primary antibody against p65 overnight at 4°C, followed by an Alexa Fluor 680-conjugated secondary antibody in the dark for 1 hour. Nuclear localization of p65 was visualized using a confocal laser scanning microscope (Carl Zeiss AG, BW, Germany).

RNA Extraction and qRT-PCR

MH7A cells were treated with quercetin at concentrations of 0, 0.5, 1, and 1.5 μmol/L, in the presence or absence of TNF-α (30 ng/mL), for 24 hours. UCB-9260 (0.5 μmol/L) and MTX (0.5 μg/mL) served as positive controls. Total RNA was extracted using the Eastep® Super Total RNA Extraction Kit and reverse-transcribed with the PrimeScript RT Master Mix kit. Quantitative PCR was performed using the SYBR Green qPCR Master Mix. Primer sequences included: *GAPDH*, FW 5′-ACAACTTTGGTATCGTGGAAGG-3′, RV 5′-GCCATCACGCCACAGTTTC-3′; *COX-2*, FW 5′-CTGGCG CTCAGCCATACAG-3′, RV 5′-CGCACTTATACTGGTCAAATCCC-3′; Inducible nitric oxide synthase (*INOS*), FW 5′-TTCAGTATCACAACCTCAGCAAG-3′, RV 5′-TGGACCTGCAAGTTAAAATCCC-3′; *IL-6*, FW 5′-CCTGAA CCTTCCAAAGATGGC-3′, RV 5′-TTCACCAGGCAAGTCTCCTCA-3′; *IL-1β*, FW 5′-TTCGACACATGGGAT AACGAGG-3′, RV 5′-TTTTTGCTGTGAGTCCCGGAG-3′. The mRNA levels were calculated using the $2^{-\Delta\Delta Ct}$ method, with *GAPDH* as an endogenous control.

CIA Rat Model and Quercetin Treatment

As reported, RA affects females 3 to 5 times more frequently than males.[15] Consequently, female Wistar rats have been extensively utilized in research pertaining to RA.[16] Female Wistar rats (specific pathogen free grade, weighing 180–200 g) were sourced from Topgene Biotechnology Co., Ltd. (Changsha, China). The animals were divided into six groups: normal (0.5% CMC-Na), model (0.5% CMC-Na), and four treatment groups receiving quercetin (25, 50, and 100 mg/kg) or MTX (0.9 mg/kg). CIA was induced using incomplete Freund's adjuvant and bovine type II collagen. Rats received treatments via intragastric administration starting on Day 0 and continuing twice weekly for four weeks.[17]

Paw Volume Analysis and ELISA

Paw volumes were measured using a PV-200 toe volume measuring instrument (Chengdu Techman Software Co., Ltd.). Rats were euthanized under deep anesthesia, and blood and ankle joints were immediately collected. Serum levels of RF, TNF-α, IL-6, and IL-1β were quantified using ELISA kits, following the manufacturer's protocols.

Pathological Analyses of Ankle Joints in CIA Rats

Ankle joints were fixed in 10% formaldehyde, decalcified in 15% EDTA, and processed for histological examination. Tissues were embedded in paraffin, sectioned, and stained with hematoxylin and eosin (H&E). The pathological changes were analyzed using a microscope.

Statistical Analysis

Error bars in the graphs indicate the mean ± standard deviation (s.d.) and were generated using GraphPad Prism software (version 8.3.0; GraphPad Software, San Diego, CA). Statistical significance was assessed using one-way analysis of variance test or Student's *t*-tests in SPSS software (version 25.0; IBM Corp., Armonk, NY, USA). Heatmaps were generated using GraphPad Prism software, and bubble plots were generated using Hiplot. Significance levels are denoted as follows: $^{*, \#, \$}p < 0.05$, $^{**, \#\#}p < 0.01$, $^{***, \$\$\$, \#\#\#}p < 0.001$.

Results

Anti-TNF-α Activity of TFPF

Given the pivotal role of TNF-α in the pathogenesis and severity of RA, as documented in recent research,[18] we investigated whether TFPF could counteract the effects of TNF-α. The total flavonoid content of both PF extract and TFPF was determined by ultraviolet spectrophotometry following the enrichment of TFPF from PF extract using D101 macroporous resin. Our analyses revealed that the total flavonoid content of PF extract and TFPF was quantified at 21.33% and 60.74%, respectively (Supplementary Figure 1). Experiments conducted with L929 cells demonstrated that PF extract and TFPF at concentrations ranging from 25 to 250 ng/mL did not compromise cell viability (Figure 1A and B). Notably, at dosages of 50 and 100 ng/mL, both PF extract and TFPF significantly enhanced the viability of L929 cells subjected to TNF-α and Act-D treatment, indicating a protective effect ($p < 0.05$, Figure 1C).

Subsequently, NlucP-NF-κB-HEK293T cells were utilized to assess the anti-TNF-α effects of PF extract and TFPF. Concentrations of PF extract and TFPF below 500 ng/mL were found to be non-toxic to HEK293T cells (Figure 1D and E). Luciferase assays demonstrated that both PF extract (250–500 ng/mL) and TFPF (100–500 ng/mL) significantly reduced luciferase activity levels ($p < 0.01$, Figure 1F). Moreover, TFPF exhibited superior efficacy compared to PF extract ($p < 0.05$, Figure 1F), implying that TFPF may serve as a crucial bioactive component in the anti-TNF-α activity of PF. These findings suggest that various constituents of the TFPF extract may possess anti-TNF-α properties.

Identification of Bioactive Compounds in TFPF

UHPLC-Q-Exactive Orbitrap HRMS was used to identify the phytochemical compounds in TFPF. The chromatograms revealed the presence of five compounds through comparison with specified standard substances and in alignment with established literature sources.[19–23] These compounds, including fisetin, glycitein, isoliquiritigenin, formononetin, and wogonin, were detected in positive ion mode (Figure 2A). Additionally, various compounds such as catechin,

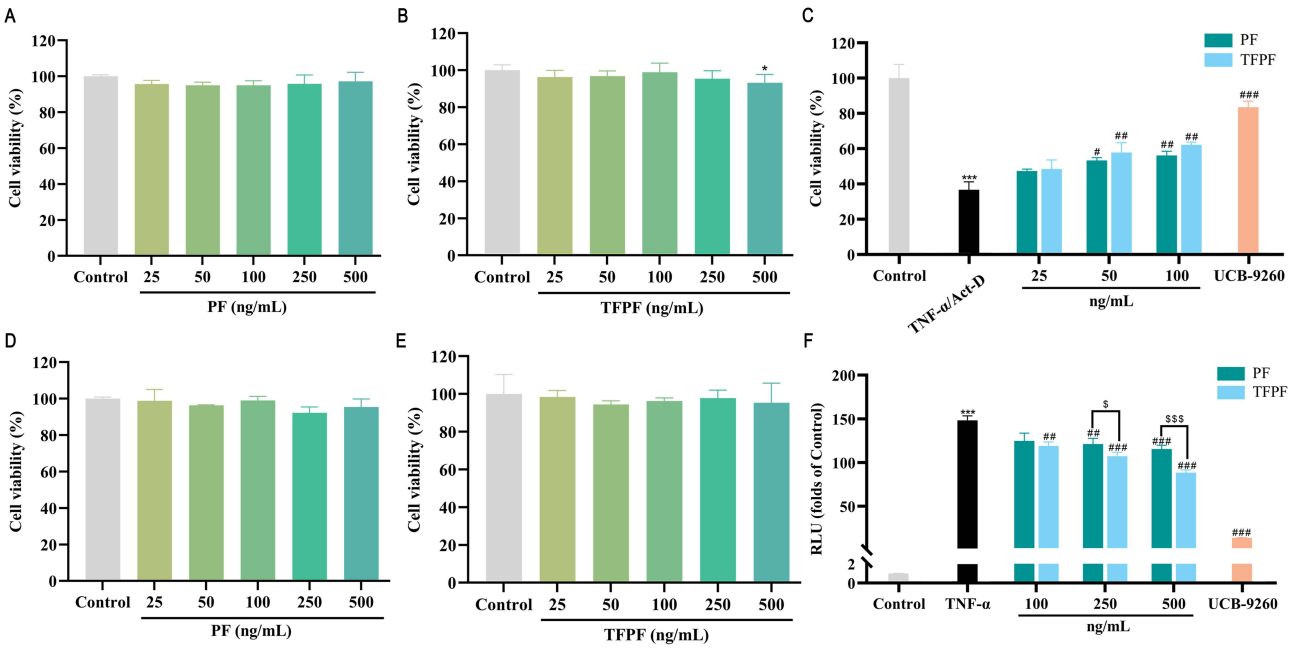

Figure 1 Anti-TNF-α Effects of TFPF. (**A** and **B**) Cell viability assays demonstrating the impact of PF extract and TFPF on L929 cells across a range of concentrations (0–500 ng/mL). (**C**) Enhanced viability of L929 cells treated with PF extract and TFPF under TNF-α/Act-D stress. (**D** and **E**) Viability of HEK293T cells following exposure to PF extract and TFPF. (**F**) Luciferase activity measured following post-treatment with PF extract and TFPF. UCB-9260 served as a positive control. Data are presented as mean ± s.d., n = 6. $^{*}p < 0.05$, $^{***}p < 0.001$ vs control group; $^{\#}p < 0.05$, $^{\#\#}p < 0.01$, $^{\#\#\#}p < 0.001$ vs TNF-α/Act-D or TNF-α group; $^{\$}p < 0.05$, $^{\$\$\$}p < 0.001$.
Abbreviation: RLU, relative light units.

procyanidin A2, and quercetin were detected under negative ion mode (Figure 2B), and their presence was validated through comparison with standard substances and existing literature sources.[24–26] Further details can be found in Table 1.

Quercetin Displays the Highest Enhancement in L929 Cell Viability Among the Eight Compounds of TFPF

In contrast to TNF-α/Act-D alone, isoliquiritigenin, wogonin, and fisetin significantly reduced cell viability ($p < 0.001$, Figure 3). Formononetin did not exhibit any noticeable effects on L929 cell viability. However, a notable increase in cell viability was observed following treatment with glycitein, catechin, procyanidin A2, and quercetin ($p < 0.001$, Figure 3), with quercetin demonstrating the most pronounced upregulation.

Quercetin Antagonizes the Effects of TNF-α

To further demonstrate the antagonistic effects of quercetin on TNF-α, cell viability, morphology, and apoptosis rates were assessed using the MTS assay, an inverted microscope and a flow cytometer. The results from the cell viability assays indicated that quercetin at concentrations below 50 μmol/L did not have adverse effects on L929 cells (Figure 4A). Notably, treatment with quercetin significantly enhanced the viability of L929 cells subjected to TNF-α ($p < 0.001$, Figure 4B) and protected these cells from TNF-α-induced fragmentation (Figure 4C) and apoptosis ($p < 0.001$, Figure 4D). These findings provide evidence that quercetin effectively counteracts the biological impact of TNF-α.

Identification of Quercetin Target

The study conducted a TPP experiment on MH7A cells to identify specific targets influenced by quercetin. Analysis of the TPP data revealed 20 DEPs distinguishing the control and quercetin-treated groups (Figure 5A). Particularly noteworthy was the remarkable stability of TNF-α. Furthermore, pathway enrichment analysis revealed a significant enrichment of the TNF signaling pathway (Figure 5B). These results imply that TNF-α could serve as a promising therapeutic target modulated by quercetin.

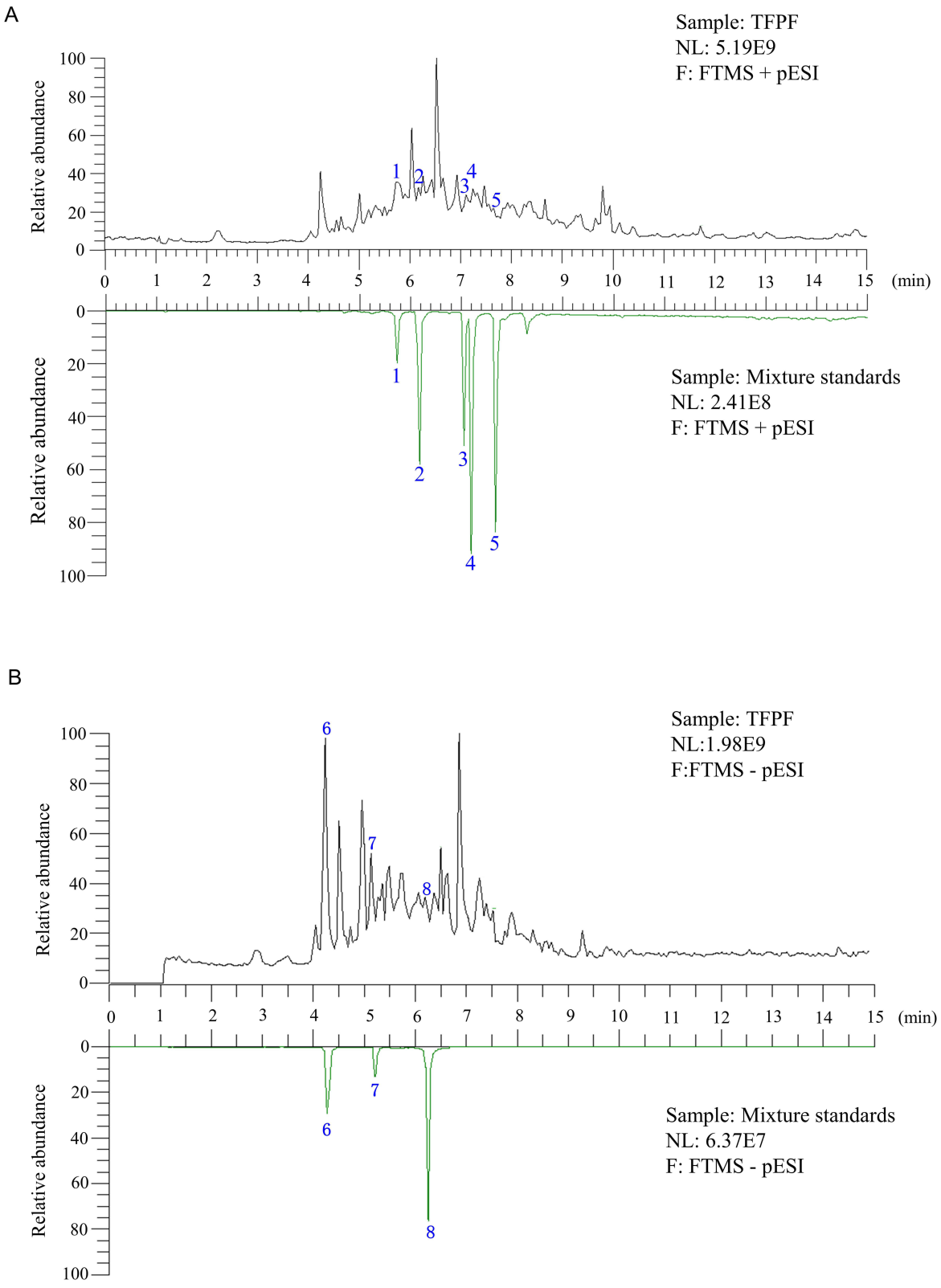

Figure 2 UHPLC-Q-Exactive Plus Orbitrap HRMS chromatograms of TFPF under positive (**A**) and negative (**B**) ion modes. Identified compounds: 1. fisetin; 2. glycitein; 3. isoliquiritigenin; 4. formononetin; 5. wogonin; 6. catechin; 7. procyanidin A2; 8. quercetin.

https://doi.org/10.2147/JIR.S497166

Table 1 Identification of Eight Compounds in TFPF

Peak No.	Name	RT (minutes)	Formula	Mass	Ion Mode	Major Product Ions (*m/z*)	Literature
1	Fisetin	5.74	$C_{15}H_{10}O_6$	287.05551	$[M+H]^+$	269.04517, 213.05505, 137.02368, 121.02856	19
2	Glycitein	6.18	$C_{16}H_{12}O_5$	285.07623	$[M+H]^+$	270.05280, 242.05783, 225.05521, 197.06009	20
3	Isoliquiritigenin	7.06	$C_{15}H_{12}O_4$	257.08127	$[M+H]^+$	239.07072, 211.07541, 147.04442, 137.02367	21
4	Formononetin	7.20	$C_{16}H_{12}O_4$	269.06109	$[M+H]^+$	254.05748, 213.09131, 197.06003, 154.06235	22
5	Wogonin	7.68	$C_{16}H_{12}O_5$	285.07614	$[M+H]^+$	270.05264, 242.05772, 179.04953, 105.03424	23
6	Catechin	4.27	$C_{15}H_{14}O_6$	289.07187	$[M-H]^-$	245.08174, 203.07069, 123.04395, 109.02825	24
7	Procyanidin A2	5.21	$C_{30}H_{24}O_{12}$	575.11951	$[M-H]^-$	449.08862, 423.07181, 285.04077, 125.02318	25
8	Quercetin	6.25	$C_{15}H_{10}O_7$	301.03571	$[M-H]^-$	257.04703, 178.99762, 151.00261, 116.92736	26

Direct and Stable Binding of Quercetin to TNF-α

To substantiate that quercetin directly interacts with TNF-α, we conducted an analysis of quercetin's active targets and simulated its docking with TNF-α. The findings indicate that quercetin can indeed bind directly to TNF-α by accessing its pocket and establishing hydrogen bonds (Figure 6A). Furthermore, we performed SPR, CETSA, and DARTS assays to validate the binding affinity between quercetin and TNF-α. The analysis of SPR data revealed an increase in the response signal with escalating quercetin concentrations, ultimately yielding a fitted K_d value of 61.76 μmol/L for quercetin (Figure 6B). Moreover, both the CETSA and DARTS assays demonstrated a noticeable rise in TNF-α expression levels following quercetin treatment within the quercetin group compared to the control group treated with DMSO (Figure 6C and D). These results provide additional evidence supporting the binding interaction between quercetin and TNF-α.

Key Enrichment Pathways Influenced by Quercetin

To explore the signaling pathways influenced by quercetin targeting TNF-α, a transcriptomic analysis was conducted on MH7A cells. Volcano plots displayed differential gene expression between the control, model, and quercetin-treated groups, revealing key regulatory changes (Figure 7A–C). A Venn diagram further identified 24 shared DEGs across these comparisons (Figure 7D). KEGG pathway analysis highlighted critical pathways affected by quercetin, including cytokine-cytokine receptor interactions, TNF signaling, and several immune-related pathways, illuminating the broad-spectrum impact of quercetin on cellular signaling (Figure 7E).

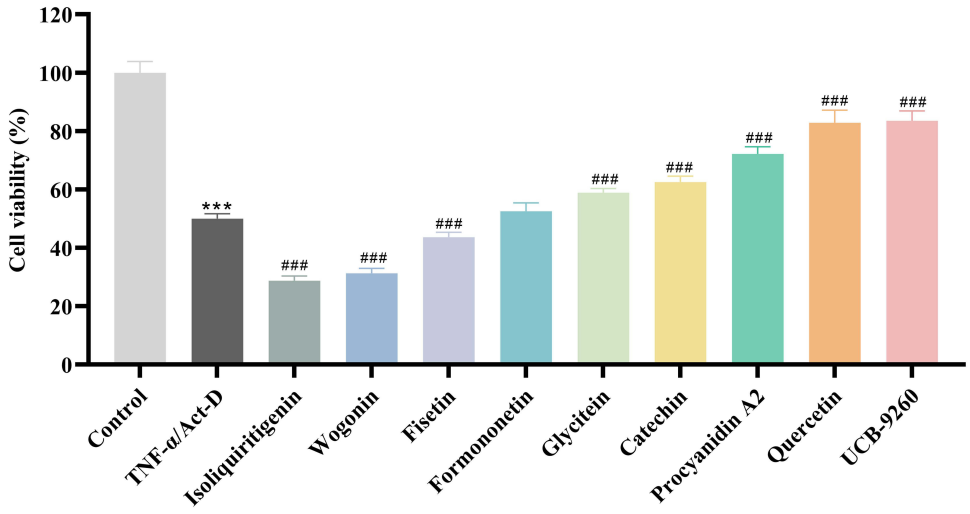

Figure 3 Cell viability of L929 cells treated with various compounds and UCB-9260 (10 μmol/L, positive control). Data are presented as mean ± s.d., n = 6. ***$p < 0.001$ vs control group; ###$p < 0.001$ vs TNF-α/Act-D group.

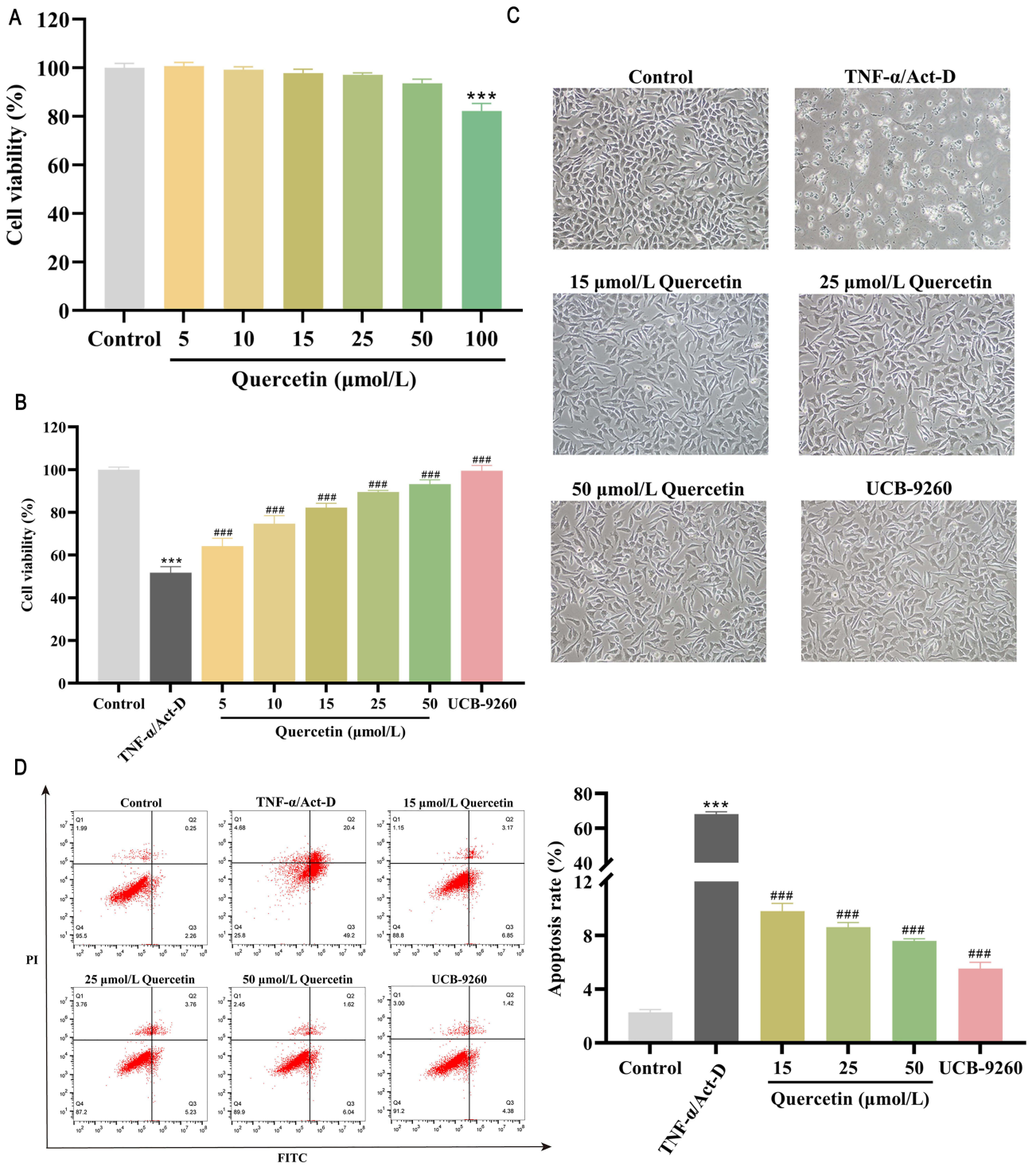

Figure 4 Quercetin's antagonistic effects on TNF-α. (**A**) Cell viability of L929 cells exposed to various concentrations of quercetin. (**B**) Enhanced viability of cells treated with quercetin in the presence of TNF-α/Act-D. (**C**) Photomicrographs depicting cellular morphology following quercetin treatment. (**D**) Apoptosis rates and flow cytometry analysis post-quercetin treatment. UCB-9260 served as a positive control. Data are presented as mean ± s.d., n = 6. ***$p < 0.001$ vs control group; ###$p < 0.001$ vs TNF-α/Act-D group.

Inhibition of the TNF-α/NF-κB Signaling Pathway by Quercetin

Transcriptomic analyses revealed the capacity of quercetin to modulate the downstream TNF signaling pathway. Given the link between the TNF signaling pathway and the activation of the NF-κB signaling pathway, as reported by Huang et al,[27] we examined the expression levels of the NF-κB signaling pathway in two cell lines to offer additional insights into the regulatory

https://doi.org/10.2147/JIR.S497166

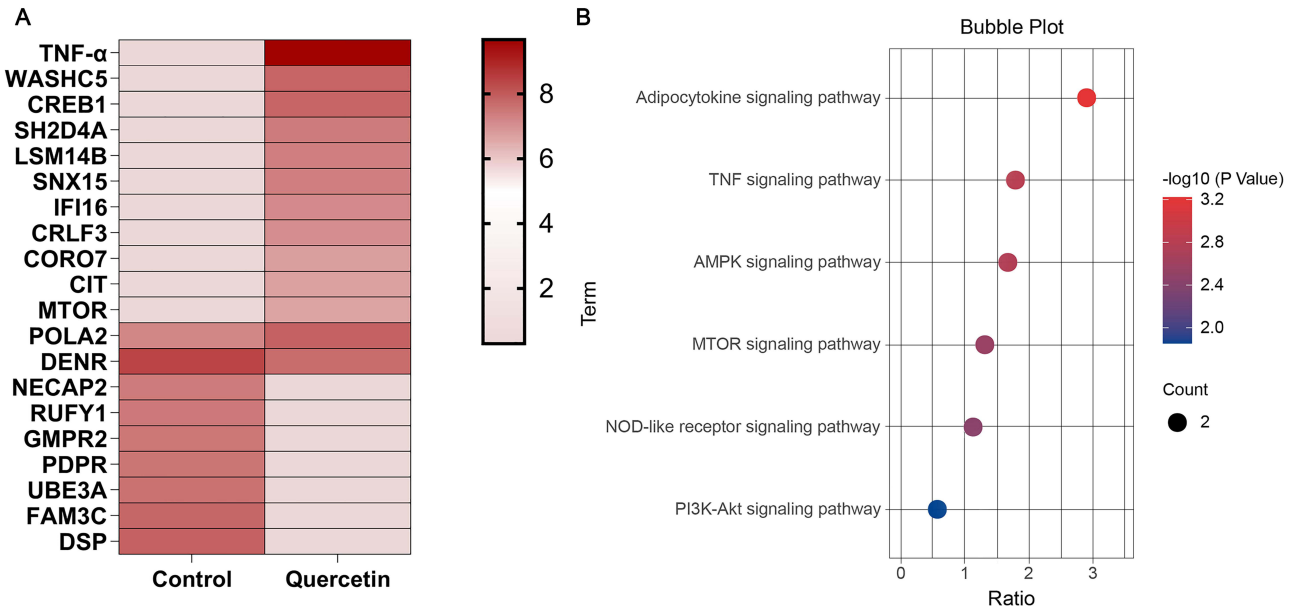

Figure 5 Heatmap of DEPs showing changes in protein stability (**A**) and KEGG pathway enrichment analysis (**B**) indicating the pathways modulated by quercetin treatment.

mechanism of quercetin. Cell viability assays demonstrated the safety of quercetin at concentrations below 50 μmol/L in HEK293T cells (Figure 8A). Treatment with TNF-α significantly increased the luciferase expression level, an effect mitigated by quercetin ($p < 0.001$, Figure 8B). Moreover, as depicted in Figure 8C, quercetin treatment below 100 μmol/L had no discernible impact on MH7A cell viability. Concurrently, quercetin treatment at concentrations of 0.5, 1, and 1.5 μmol/L markedly decreased TNF-α-induced relative expression levels of p-p65/p65 and p-IκBα/IκBα ($p < 0.001$, Figure 8D–F), p65 nuclear translocation (Figure 8G), and mRNA levels of downstream inflammatory factors (*COX-2, INOS, IL-6*, and *IL-1β*) to levels approaching normal ($p < 0.05$, Figure 9A–D). Taken together, these findings provide compelling evidence that quercetin effectively inhibits the activation of the TNF-α/NF-κB signaling pathway.

Quercetin Protects Rats From RA

The results obtained in vitro clearly demonstrate that quercetin exhibits a strong binding affinity and inhibitory effect on TNF-α activity, leading to downregulation of the TNF-α/NF-κB signaling pathway. Subsequently, we investigated the potential of quercetin to mitigate RA in a rat model. Our hypothesis centered on the presumed anti-RA properties of quercetin in vivo. Consistent with our expectations, histological examination by H&E staining revealed a reversal of the inflammatory damage to articular cartilage following quercetin treatment (Figure 10A). Notably, quercetin treatment significantly reduced foot swelling (Figure 10B), paw volume ($p < 0.001$, Figure 10C), serum RF levels ($p < 0.01$, Figure 10D), and the levels of pro-inflammatory cytokines (TNF-α, IL-6, and IL-1β, $p < 0.01$, Figure 10E–G) in the experimental rats. Taken together, these observations strongly support the conclusion that quercetin exerts anti-RA effects.

Discussion

The inhibition of TNF-α activity is recognized as a pivotal strategy for modulating immune responses in RA, with the potential to significantly improve treatment outcomes.[28] Natural compounds, particularly small-molecule inhibitors, have emerged as promising therapeutic agents owing to their ability to modulate biological pathways with minimal side effects. In this context, our study contributes to the expanding field by identifying quercetin, a bioactive compound of TFPF, as a natural and novel inhibitor of TNF-α.

TNF-α is a pleiotropic cytokine known for its cytotoxic effects, particularly in L929 cells, which are highly susceptible to TNF-α-induced cytotoxicity.[29] The TNF-α-induced cell injury model is widely adopted for screening potential TNF-α inhibitors.[30] Additionally, the luciferase reporter assay offers advantages such as high sensitivity, rapid

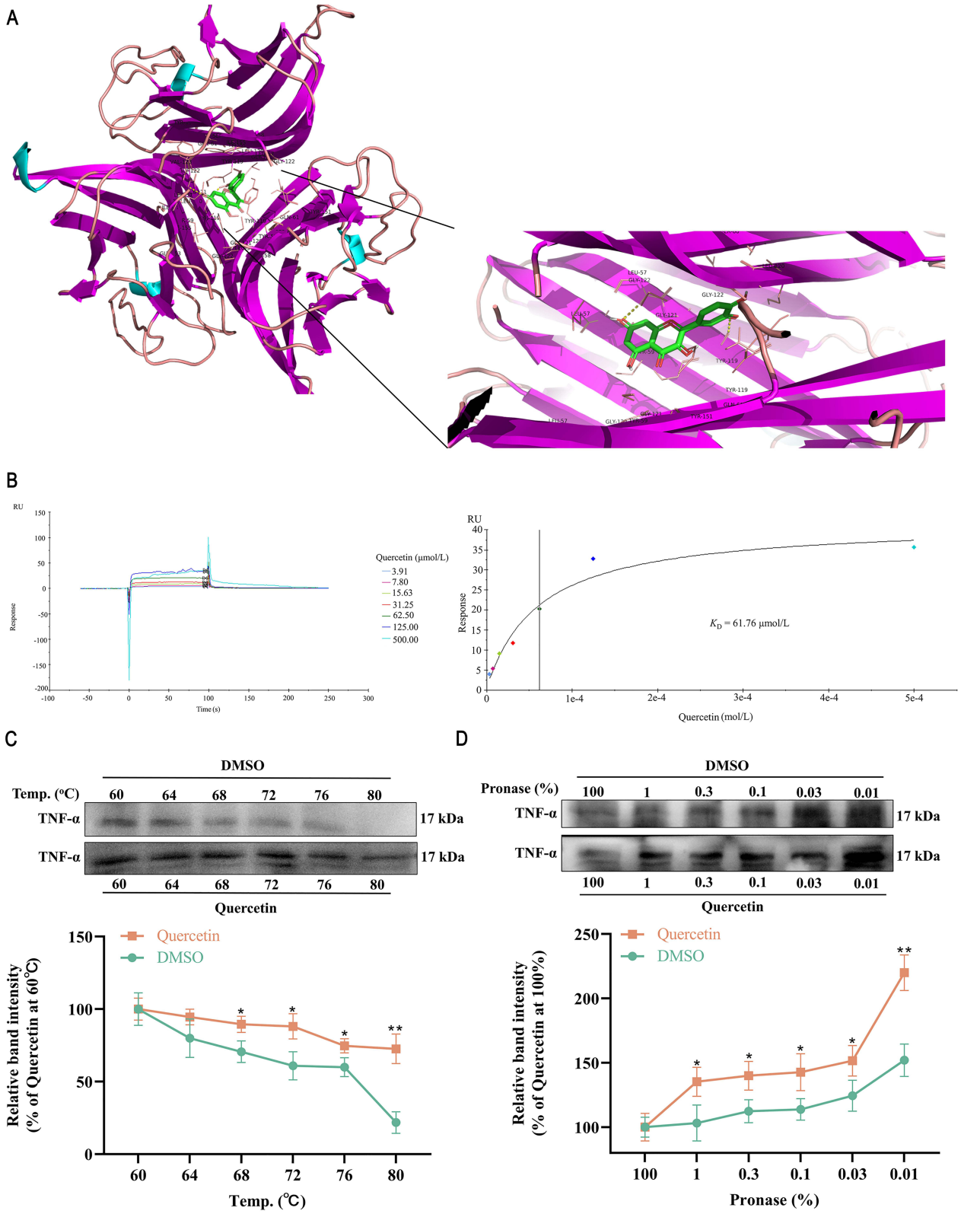

Figure 6 Quercetin binds to TNF-α directly and stably. (**A**) Molecular docking analysis of active targets in the structure of quercetin and TNF-α crystal structure. (**B**–**D**) SPR affinity assay, CETSA, and DARTS analysis of the binding effect between quercetin and TNF-α. *p < 0.05, **p < 0.01 vs the corresponding DMSO-treated group.

https://doi.org/10.2147/JIR.S497166

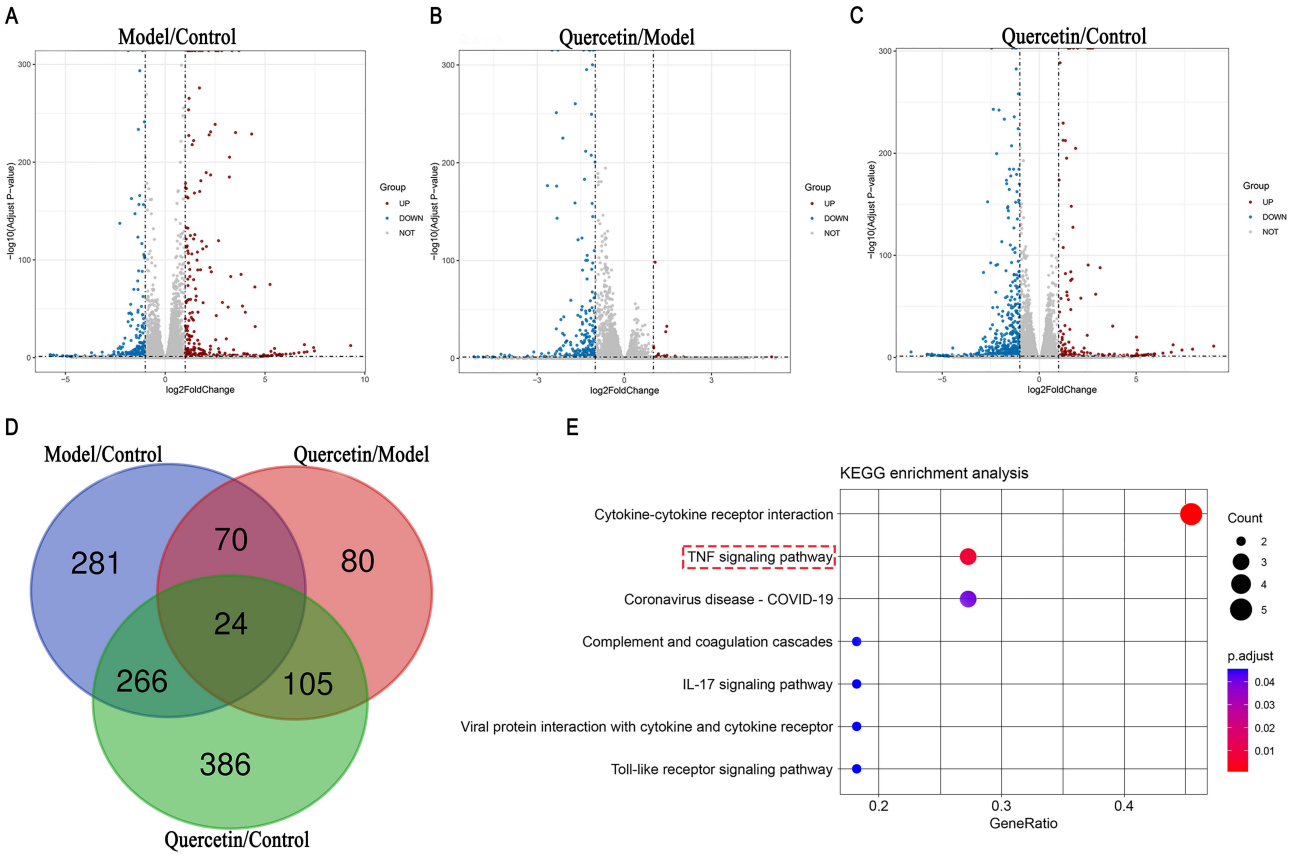

Figure 7 Overview of transcriptomic changes and pathway analysis. (**A**–**C**) Volcano plots of DEGs. (**D**) Venn diagram of shared DEGs. (**E**) KEGG pathway enrichment.

response, non-radioactivity, and stability, making it an ideal method for analyzing the antagonistic effects of small molecules on TNF-α.[31] Our study found that both PF extract and TFPF enhanced the survival of L929 cells under TNF-α challenge and reduced luciferase expression in NlucP-NF-κB-HEK293T cells, with TFPF exhibiting superior anti-TNF-α activity compared to PF extract. This suggests that TFPF represents a critical anti-TNF-α fraction of PF.

The UHPLC-Q-Exactive Orbitrap HRMS analysis, alongside an L929 cell model, facilitated the screening of TFPF compounds for their anti-TNF-α activities. Initial assessments of the eight identified compounds revealed that quercetin, procyanidin A2, catechin, and glycitein significantly inhibited TNF-α activity. Quercetin was the most potent among these, underscoring its potential as a powerful TNF-α antagonist. Quercetin, a well-known dietary supplement, has demonstrated antioxidant, anti-inflammatory, antibacterial, and anti-apoptotic properties, exhibiting significant therapeutic potential and clinical efficacy.[32,33] However, few studies have elucidated the effects of quercetin on TNF-α. In this study, we further found that quercetin treatment significantly increased cell viability, which had been drastically decreased by TNF-α, while it exerted the opposite effect on TNF-α-induced cell fragmentation and apoptosis rates. This finding confirms that quercetin possesses the property of inhibiting TNF-α, thereby deepening our understanding of the beneficial effects of quercetin.

TPP has recently emerged as a critical tool in the field of target identification for natural products, offering robust insights into the interaction dynamics between biomolecules and potential therapeutic agents.[34] The TPP analysis revealed that TNF-α exhibited significantly increased stability in the presence of quercetin compared to the DMSO control, suggesting a direct interaction between quercetin and TNF-α.

To further delineate this interaction, we employed a suite of sophisticated methodologies, including molecular docking, SPR, CETSA, and DARTS. Molecular docking is a computational method for predicting of ligand binding to receptors.[35] SPR has been used for affinity capacity analysis between two or more biomolecule interactions.[36] Molecular docking predicted quercetin's binding within the active site of TNF-α, indicating a potential inhibitory effect on this cytokine. This prediction was substantiated by SPR, which confirmed quercetin's binding affinity to TNF-α. CETSA and

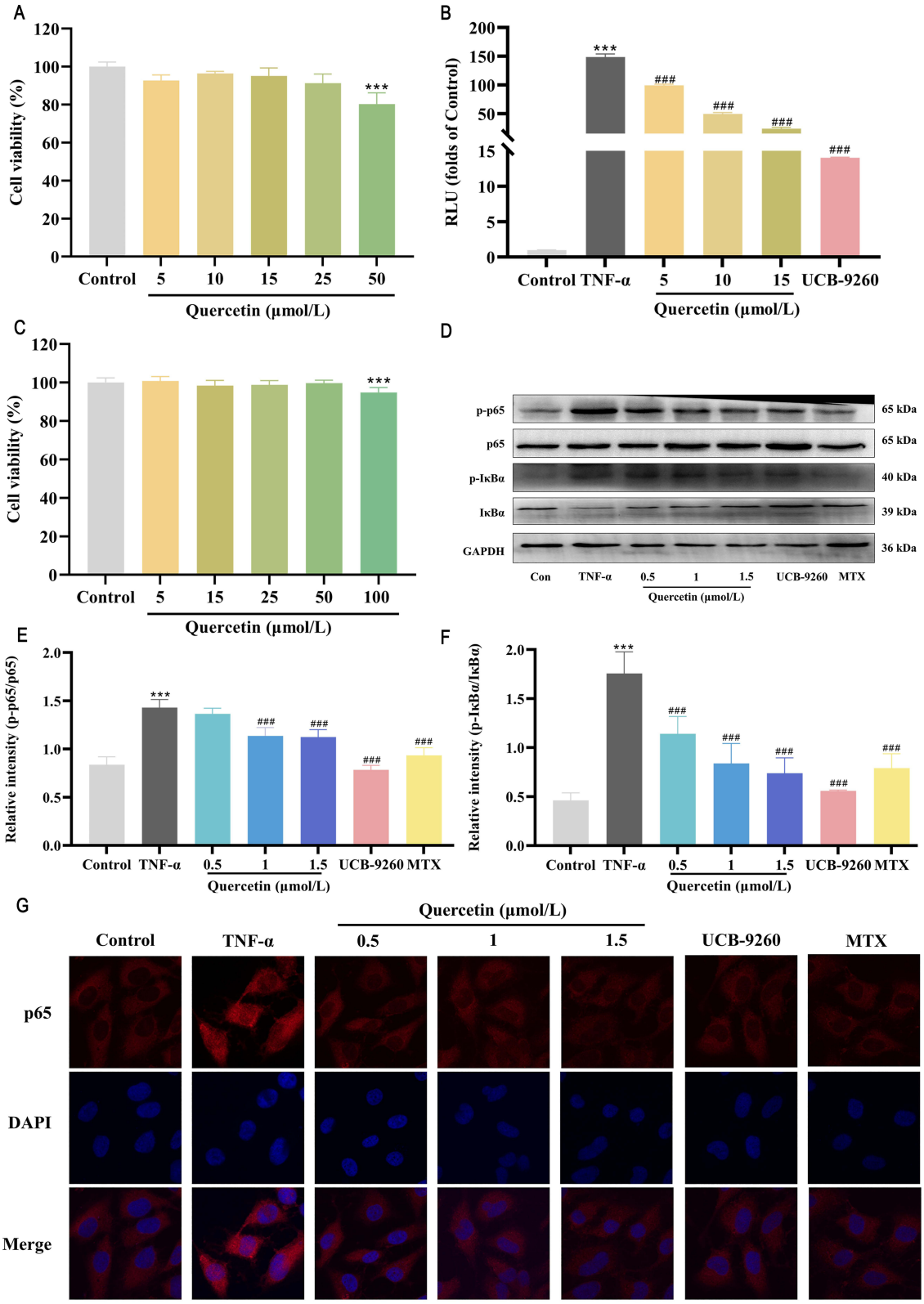

Figure 8 Impact of quercetin on the TNF-α/NF-κB signaling pathway. (**A**) Cell viability in HEK293T cells treated with varying concentrations of quercetin. (**B**) Modulation of luciferase expression by quercetin. (**C**) Cell viability in MH7A cells exposed to quercetin. (**D–F**) Representative immunoblots and relative intensity of p-p65, p65, p-IκBα, and IκBα proteins with GAPDH as the loading control. (**G**) Confocal microscopy images of p65 translocation. Data are presented as mean ± s.d., n = 6. ***$p < 0.001$ vs control group; ###$p < 0.001$ vs TNF-α group.

Abbreviation: RLU, relative light units.

https://doi.org/10.2147/JIR.S497166

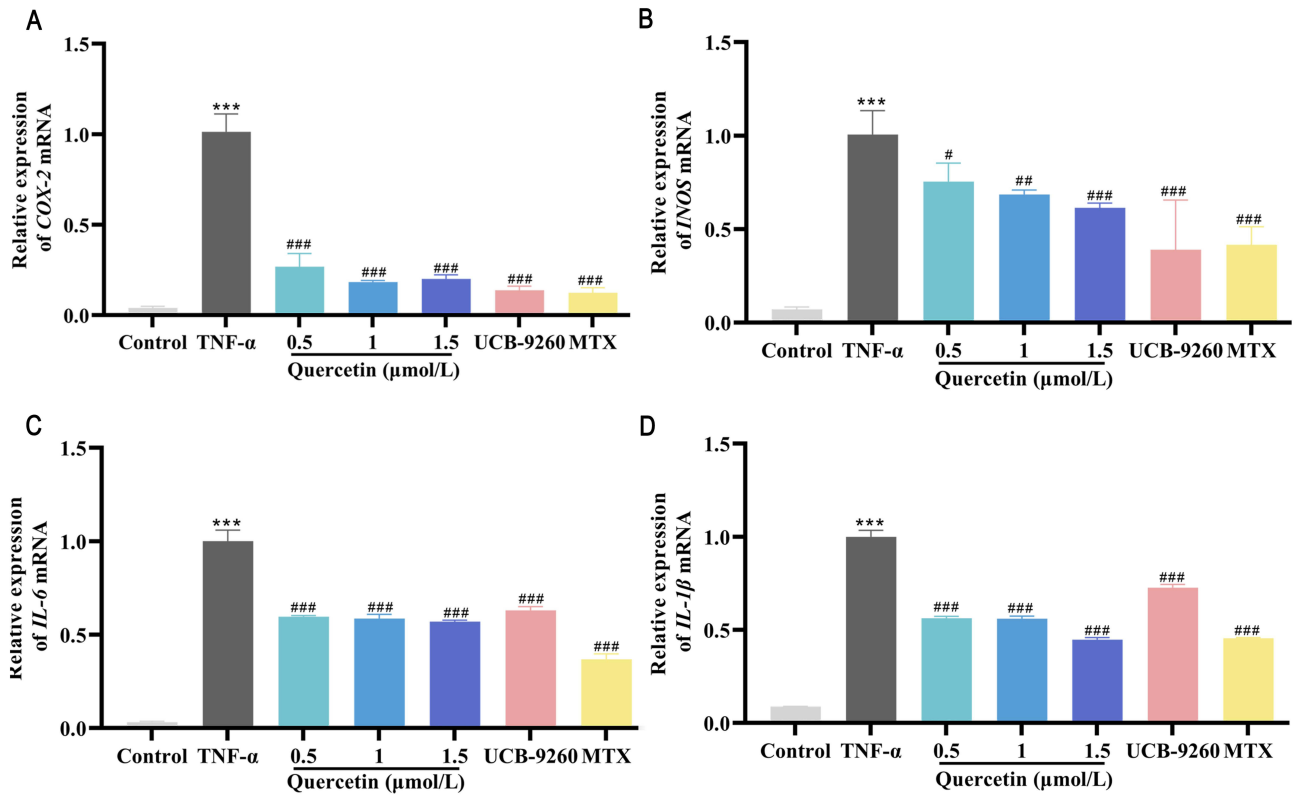

Figure 9 Effect of quercetin on inflammatory mediators in MH7A cells. Changes in mRNA levels of *COX-2* (**A**), *INOS* (**B**), *IL-6* (**C**), and *IL-1β* (**D**) post-treatment. Data are presented as mean ± s.d., n = 6. ***$p < 0.001$ vs control group; $^{\#}p < 0.05$, $^{\#\#}p < 0.01$, $^{\#\#\#}p < 0.001$ vs TNF-α group.

DARTS are based on the principle that the protein target transitions to a low energy and high stability after the small molecule drug binds to the protein target, thereby improving the thermal stability and enzyme stability of the protein target, and can directly monitor the binding stability between the small molecule drug and the protein target.[37,38] CETSA and DARTS further validated these findings, demonstrating that quercetin enhances the thermal and enzymatic stability of TNF-α, a hallmark of effective binding. The stability of the quercetin-TNF-α complex under conditions of elevated temperature or in the presence of proteases suggests a strong and stable interaction, underscoring the potential of quercetin as a potent anti-TNF-α agent.

TNF-α contributes to the worsening of inflammation and the resultant destruction of joints and cartilage, thereby perpetuating a detrimental cycle of tissue damage.[39,40] Our study elucidates the molecular interactions involving quercetin and its targeted inhibitory effects on TNF-α. Through transcriptomic analysis, we identified specific signaling pathways affected by quercetin's modulation of TNF-α activity. Enrichment pathway analysis indicated that the TNF signaling pathway is predominantly influenced by quercetin. TNF-α binding to TNFR1 leads to the activation of the NF-κB signaling pathway, a central mechanism in the regulation of immune and inflammatory processes.[41] To assess the functional impact of quercetin on this pathway, we conducted a luciferase-based reporter gene assay and TNF-α-stimulated MH7A cells. The results were compelling: quercetin markedly inhibited luciferase expression indicative of NF-κB activity. Additionally, it effectively reduced the phosphorylation levels of IκBα and p65, crucial mediators in the NF-κB signaling cascade. This inhibition also prevented the nuclear translocation of p65, thereby reducing the transcription of pro-inflammatory genes such as *COX-2, INOS, IL-6*, and *IL-1β*. These findings underscore quercetin's capability to attenuate the activation of the TNF-α/NF-κB signaling pathway.

In addition to previous studies that have highlighted the therapeutic potential of quercetin for treating RA,[16,42] our research provides further evidence supporting its efficacy. We found that quercetin supplementation significantly alleviated symptoms in a CIA rat model, including reduced foot swelling, paw volume, and pathological changes in the ankle. Moreover, quercetin treatment effectively normalized serum levels of RF, IL-6, IL-1β, and TNF-α. These

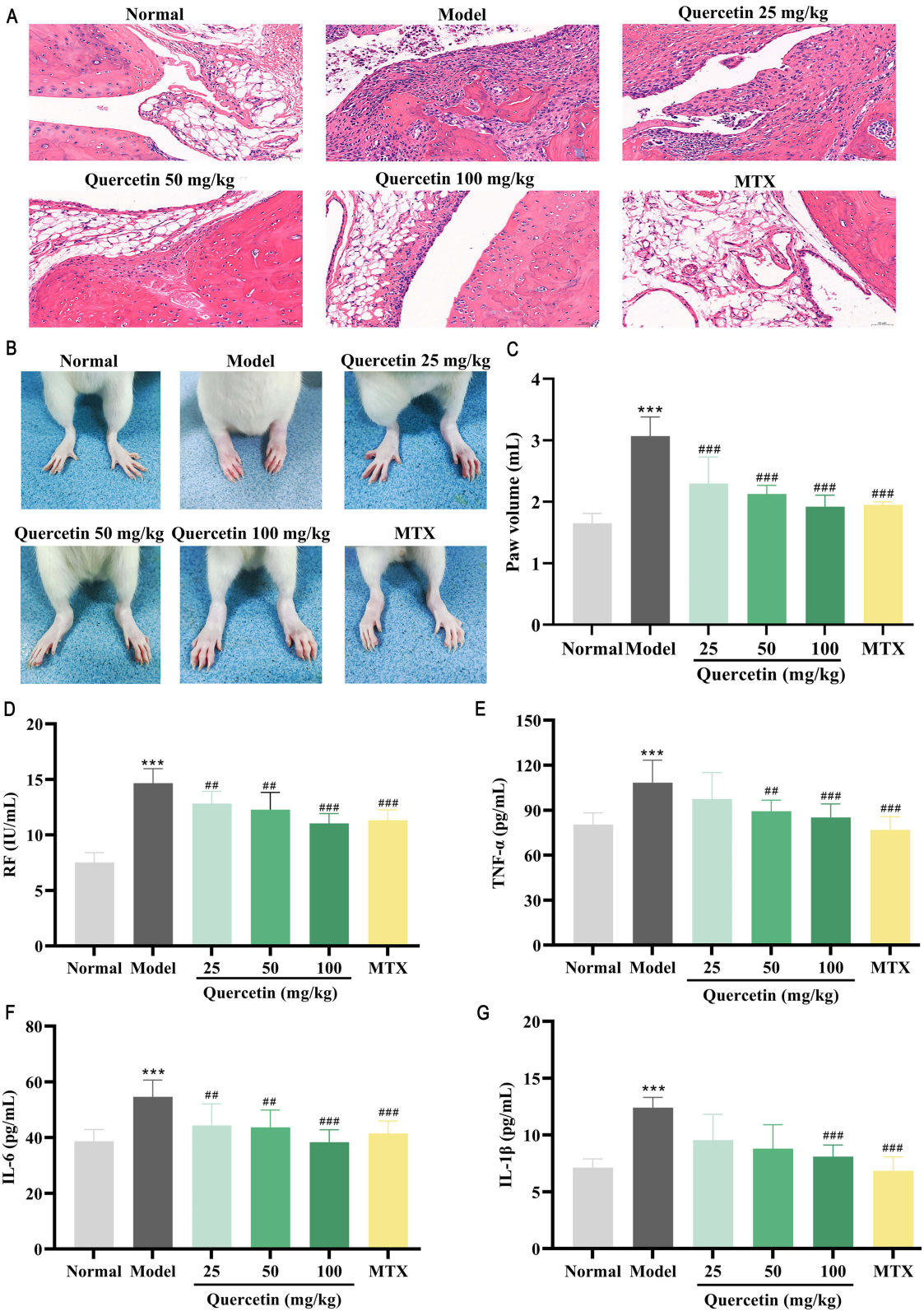

Figure 10 Quercetin protects rats from RA. (**A**) Articular cartilage tissue was collected after quercetin (25, 50, and 100 mg/kg) treatment for H&E staining (200 ×, Scale bar = 50 μm). (**B**) Representative photographs of foot swelling. (**C**) Paw volume in the rats. (**D**–**G**) Serum levels of RF, TNF-α, IL-6, and IL-1β after quercetin (25, 50, and 100 mg/kg) treatment. MTX (0.9 mg/kg) was used as a positive control. Data are presented as mean ± s.d., n = 6. ***$p < 0.001$ vs normal group; $^{\#\#}p < 0.01$, $^{\#\#\#}p < 0.001$ vs model group.

https://doi.org/10.2147/JIR.S497166

findings confirm the ability of quercetin to modulate key biomarkers associated with RA pathology. Collectively, these results underscore the potential of quercetin as a potent anti-RA agent, offering a natural alternative that could complement existing therapeutic strategies for managing RA.

Despite the promising results presented, our study has several limitations that warrant consideration. First, we focused primarily on quercetin and did not explore other potential anti-TNF-α compounds. This leaves open the possibility of further investigation into additional bioactive compounds that may contribute synergistically to its anti-RA effects. Second, although our results indicate a strong interaction between quercetin and TNF-α, the specific binding mechanisms remain to be fully elucidated at the molecular level, necessitating more comprehensive experimental investigation in future studies.

Conclusion

In conclusion, our study provides compelling evidence that quercetin, identified as a promising natural TNF-α inhibitor of TFPF, effectively binds to and inhibits TNF-α, thereby modulating the TNF-α/NF-κB signaling pathway. Furthermore, we report a groundbreaking discovery that quercetin exhibits anti-RA properties through its specific targeting of TNF-α. This novel insight not only enhances the edible and therapeutic potential of quercetin in various clinical settings but also contributes valuable methodologies for investigating molecular targets in edible and medicinal plants and their bioactive compounds.

Abbreviations

Act-D, actinomycin D; BSA, bovine serum albumin; CETSA, cellular thermal shift assay; CIA, collagen-induced arthritis; COX-2, cyclooxygenase-2; DARTS, drug affinity responsive target stability; DMEM, Dulbecco's modified Eagle medium; DMSO, dimethyl sulfoxide; ELISA, enzyme-linked immunosorbent assay; GAPDH, glyceraldehyde-3-phosphate dehydrogenase; H&E, hematoxylin and eosin; IL-1β, interleukin-1β; IL-6, interleukin-6; INOS, inducible nitric oxide synthase; L929, mouse fibroblast cell line; LPS, lipopolysaccharide; MTX, methotrexate; PBS, phosphate buffered saline; PF, *Periploca forrestii* Schltr.; PMSF, phenylmethanesulfonyl fluoride; RA, rheumatoid arthritis; RF, rheumatoid factor; RIPA, radio immunoprecipitation assay; RLU, relative light units; RPMI, Roswell Park Memorial Institute; SPR, surface plasmon resonance; TFPF, total flavonoids of *Periploca forrestii* Schltr.; TNF-α, tumor necrosis factor alpha; TPP, Thermal proteome profiling.

Data Sharing Statement

Data will be made available on request. The transcriptomic data have been deposited in the Sequence Read Archive database (PRJNA1106215).

Ethics Statement

The research protocol was approved by the Animal Care Welfare Committee of Guizhou Medical University (protocol code No. 2000824 and date of 1 April 2020). All experiments and procedures were performed according to the National Institutes of Health Guide for the Care and Use of Laboratory Animals (NIH Publications No. 8023, revised 1978).

Author Contributions

All authors made a significant contribution to the work reported, whether that is in the conception, study design, execution, acquisition of data, analysis and interpretation, or in all these areas; took part in drafting, revising or critically reviewing the article; gave final approval of the version to be published; have agreed on the journal to which the article has been submitted; and agree to be accountable for all aspects of the work.

Funding

This work was supported by the National Natural Science Foundation of China (No. 82060703); the Guizhou Provincial Basic Research Program (Natural Science) (Nos. ZK[2022] key 037 and [2021]5619); the Guizhou Provincial Health Commission (No. 2024GZYXKYJJXM0133); and the Guizhou Science and Technology Department (No. [2023]006).

Disclosure

The authors state no competing interests in this work.

References

1. Ansari UAMA, Uddin Q, Husain N, Ahmad T, Fatima SH, Minhajuddin A. Evaluation of the efficacy and safety of a herbal formulation for rheumatoid arthritis—a non-inferiority randomized controlled trial. *J Ethnopharmacol*. 2024;325:117833. doi:10.1016/j.jep.2024.117833
2. Liu M, Wang J, Chen S-M, et al. Exploring the effect of Er miao San-containing serum on macrophage polarization through miR-33/NLRP3 pathway. *J Ethnopharmacol*. 2023;307:116178. doi:10.1016/j.jep.2023.116178
3. Zheng J, Zeng P-Y, Zhang H-T, et al. Long noncoding RNA ZFAS1 silencing alleviates rheumatoid arthritis via blocking miR-296-5p-mediated down-regulation of MMP-15. *Int Immunopharmacol*. 2021;90:107061. doi:10.1016/j.intimp.2020.107061
4. Finckh A, Gilbert B, Hodkinson B, et al. Global epidemiology of rheumatoid arthritis. *Nat Rev Rheumatol*. 2022;18(10):591–602. doi:10.1038/s41584-022-00827-y
5. Lin YJ, Anzaghe M, Schülke S. Update on the pathomechanism, diagnosis, and treatment options for rheumatoid arthritis. *Cells*. 2020;9(4):880. doi:10.3390/cells9040880
6. Brenner D, Blaser H, Mak TW. Regulation of tumour necrosis factor signalling: live or let die. *Nat Rev Immunol*. 2015;15(6):362–374. doi:10.1038/nri3834
7. Xue H-Y, Liu M-W, Yang G. Resveratrol suppresses lipopolysaccharide-mediated activation of osteoclast precursor RAW 264.7 cells by increasing miR-181a-5p expression. *Int J Immunopathol Pharmacol*. 2023;37:03946320231154995. doi:10.1177/03946320231154995
8. Shi D-C, Wang P-Y, Xu L, et al. Potential of Dendrobium officinale oligosaccharides to alleviate chronic colitis by modulating inflammation and gut microbiota. *Food Med Homol*. 2025;2:9420077. doi:10.26599/FMH.2025.9420077
9. Zhang H-T, Shi N, Diao Z, Chen Y-H, Zhang Y-J. Therapeutic potential of TNFα inhibitors in chronic inflammatory disorders: past and future. *Genes Dis*. 2021;8(1):38–47. doi:10.1016/j.gendis.2020.02.004
10. Fan H-Y, Gao Z-F, Ji K, et al. The in vitro and in vivo anti-inflammatory effect of osthole, the major natural coumarin from *Cnidium monnieri* (L.) Cuss, via the blocking of the activation of the NF-κB and MAPK/p38 pathways. *Phytomedicine*. 2019;58:152864. doi:10.1016/j.phymed.2019.152864
11. Chen L, Tang S-Q, Li X-J, et al. A review on traditional usages, chemical constituents and pharmacological activities of periploca forrestii schltr. *J Ethnopharmacol*. 2021;271:113892. doi:10.1016/j.jep.2021.113892
12. Liu T, Wang X, He Y-L, et al. In vivo and in vitro anti-arthritic effects of cardenolide-rich and caffeoylquinic acid-rich fractions of *Periploca forrestii*. *Molecules*. 2018;23(8):1988. doi:10.3390/molecules23081988
13. Cao -T-T, Yang C, Sun J, et al. Effective components of periploca forrestii against rheumatoid arthritis by targeting TNF-α. *Chin J Exp Tradit Med Formulae*. 2022;28(03):187–195. doi:10.13422/j.cnki.syfjx.20220211
14. Liu Z-H, Zhai J-X, Han N, Jun Y. Assessment of anti-diabetic activity of the aqueous extract of leaves of Astilboides tabularis. *J Ethnopharmacol*. 2016;194:635–641. doi:10.1016/j.jep.2016.10.003
15. Radu AF, Bungau SG. Management of rheumatoid arthritis: an overview. *Cells*. 2021;10(11):2857. doi:10.3390/cells10112857
16. Liu X-R, Tao T, Yao H, Zheng H-L, Wang F-M, Gao Y-X. Mechanism of action of quercetin in rheumatoid arthritis models: meta-analysis and systematic review of animal studies. *Inflammopharmacology*. 2023;31(4):1629–1645. doi:10.1007/s10787-023-01196-y
17. Wu -S-S, Xu -X-X, Shi -Y-Y, et al. System pharmacology analysis to decipher the effect and mechanism of active ingredients combination from herb couple on rheumatoid arthritis in rats. *J Ethnopharmacol*. 2022;288:114969. doi:10.1016/j.jep.2022.114969
18. Meng M, Wang L-F, Yao Y, et al. *Ganoderma lucidum* polysaccharide peptide (GLPP) attenuates rheumatic arthritis in rats through inactivating NF-κB and MAPK signaling pathways. *Phytomedicine*. 2023;119:155010. doi:10.1016/j.phymed.2023.155010
19. Sun J-F, Dong W-T, Chen L-Y, Sun G-D, Huo J-H, Wang W-M. Analysis of chemical constituents of Ginseng-Douchi compound fermentation products based on UPLC-Q-TOF-MS. *China J Chin Mater Med*. 2021;46(06):1417–1429. doi:10.19540/j.cnki.cjcmm.20210223.301
20. Liu Y-L, Wei S-F, Song Y-G, et al. Metabolism of Formononetin in *Millettia nitida Benth. var. hirsutissima Z. Wei* extract co-incubated with rat intestinal flora by UPLC/Q-TOF-MS/MS. *Chin J New Drugs*. 2015;24(23):2715–2723.
21. Luo Y, Wang C-Q, Gong Z-P, et al. Analysis of chemical compositions in miao medicine *Caesalpinia decapetala* by UPLC-Q-TOF-MS/MS. *China Pharm*. 2020;31(20):2481–2486. doi:10.6039/j.issn.1001-0408.2020.20.09
22. Chen H-X, Zhou H, Tao R, Qi Z-W, Li W-J, Wang C-Z. Study on polyphenols in lacquer tree by matrix solid-phase dispersion and HPLC-IT-TOF /MS. *Chem Ind For Prod*. 2022;42(01):10–20. doi:10.3969/j.issn.0253-2417.2022.01.002
23. Zhang -Y-Y, Zhang S-Q, Long Y-L, et al. Stimulation of hair growth by Tianma Gouteng decoction: identifying mechanisms based on chemical analysis, systems biology approach, and experimental evaluation. *Front Pharmacol*. 2022;13:1073392. doi:10.3389/fphar.2022.1073392
24. Gudžinskaitė I, Stackevičienė E, Liaudanskas M, et al. Variability in the qualitative and quantitative composition and content of phenolic compounds in the fruit of introduced American Cranberry (*Vaccinium macrocarpon* Aiton). *Plants*. 2020;9(10):1379. doi:10.3390/plants9101379
25. Qu X-W, Xiang X-L, Gao T-X, Song C-W. Determination of catechins in Fuzhuan Brick-Tea before and after fermentation by liquid chromatography mass spectrometry. *J Hubei Univ Chin Med*. 2022;24(05):43–47. doi:10.3969/j.issn.1008987x.2022.05.10
26. Wang Y, Gu Y-T, Ding Z-H, et al. Identification and analysis of quercetin and its glycosides in Rosa Roxburghii by ultra high performance liquid chromatography-tandem high resolution mass spectrometry. *Chin J Anal Chem*. 2020;48(07):955–961. doi:10.19756/j.issn.0253-3820.191338
27. Huang Z-H, Wu C, Zhou W, et al. Compound Kushen Injection inhibits epithelial-mesenchymal transition of gastric carcinoma by regulating VCAM1 induced by the TNF signaling pathway. *Phytomedicine*. 2023;118:154984. doi:10.1016/j.phymed.2023.154984
28. Fernandez CA. Pharmacological strategies for mitigating anti-TNF biologic immunogenicity in rheumatoid arthritis patients. *Curr Opin Pharmacol*. 2023;68:102320. doi:10.1016/j.coph.2022.102320
29. Vanlangenakker N, Bertrand MJM, Bogaert P, Vandenabeele P, Vanden Berghe T. TNF-induced necroptosis in L929 cells is tightly regulated by multiple TNFR1 complex I and II members. *Cell Death Dis*. 2011;2(11):e230. doi:10.1038/cddis.2011.111
30. Lai X-Y, Wei J, Ding X-H. Paeoniflorin antagonizes TNF-α-induced L929 fibroblastoma cells apoptosis by inhibiting NF-κBp65 activation. *Dose Response*. 2018;16(2):1559325818774977. doi:10.1177/1559325818774977

31. Lee D, Kim J-W, Lee C-Y, et al. *Guettarda crispiflora* Vahl methanol extract ameliorates acute lung injury and gastritis by suppressing Src phosphorylation. *Plants*. 2022;11(24):3560. doi:10.3390/plants11243560
32. Lu S-Y, Dan L-T, Sun -S-S, Fu T, Chen J. Dietary quercetin intake is associated with lower ulcerative colitis risk but not Crohn's disease in a prospective cohort study and *in vivo* experiments. *Food Funct*. 2024;15(12):6553–6564. doi:10.1039/d3fo05391a
33. Devi V, Deswal G, Dass R, et al. Therapeutic potential and clinical effectiveness of quercetin: a dietary supplement. *Recent Adv Food Nutr Agric*. 2024;15(1):13–32. doi:10.2174/012772574x269376231107095831
34. Tu Y-B, Tan L-H, Tao H-X, Li Y-F, Liu H-Q. CETSA and thermal proteome profiling strategies for target identification and drug discovery of natural products. *Phytomedicine*. 2023;116:154862. doi:10.1016/j.phymed.2023.154862
35. Zhao S-H, Zhang -P-P, Yan Y-H, et al. Network pharmacology-based prediction and validation of the active ingredients and potential mechanisms of the Huangxiong formula for treating ischemic stroke. *J Ethnopharmacol*. 2023;312:116507. doi:10.1016/j.jep.2023.116507
36. Lee T-H, Hirst D-J, Kulkarni K, Del Borgo M-P, Aguilar M-I. Exploring molecular-biomembrane interactions with surface plasmon resonance and dual polarization interferometry technology: expanding the spotlight onto biomembrane structure. *Chem Rev*. 2018;118(11):5392–5487. doi:10.1021/acs.chemrev.7b00729
37. Martinez Molina D, Jafari R, Ignatushchenko M, et al. Monitoring drug target engagement in cells and tissues using the cellular thermal shift assay. *Science*. 2013;341(6141):84–87. doi:10.1126/science.1233606
38. Rodriguez-Furlan C, Zhang C-H, Raikhel N, Hicks GR. Drug Affinity Responsive Target Stability (DARTS) to resolve protein-small molecule interaction in Arabidopsis. *Curr Protoc Plant Biol*. 2017;2(4):370–378. doi:10.1002/cppb.20062
39. Sun J, Zhou Z-Y, Zhou Y, et al. Anti-rheumatoid arthritis pharmacodynamic substances screening of *Periploca forrestii* Schltr.: component analyses in vitro and in vivo combined with multi-technical metabolomics. *Int J Mol Sci*. 2023;24(18):13695. doi:10.3390/ijms241813695
40. Zhu C, Wen S, Li J-Y, et al. FTY720 inhibits the development of collagen-induced arthritis in mice by suppressing the recruitment of $CD4^+$ T lymphocytes. *Drug Des Devel Ther*. 2021;15:1981–1992. doi:10.2147/dddt.S293876
41. Jiang Y-P, Zheng Y-F, Dong Q, et al. Metabolomics combined with network pharmacology to study the mechanism of Shentong Zhuyu decoction in the treatment of rheumatoid arthritis. *J Ethnopharmacol*. 2022;285:114846. doi:10.1016/j.jep.2021.114846
42. Long Z-Y, Xiang W, He Q, et al. Efficacy and safety of dietary polyphenols in rheumatoid arthritis: a systematic review and meta-analysis of 47 randomized controlled trials. *Front Immunol*. 2023;14:1024120. doi:10.3389/fimmu.2023.1024120